Published in final edited form as:
Biomaterials. 2015 January ; 37: 456–468. doi:10.1016/j.biomaterials.2014.10.044.

Telodendrimer nanocarrier for co-delivery of paclitaxel and cisplatin: A synergistic combination nanotherapy for ovarian cancer treatment

Liqiong Cai[#a,b], **Gaofei Xu**[#a,c], **Changying Shi**[a], **Dandan Guo**[a], **Xu Wang**[a], and **Juntao Luo**[a,*]

[a] Department of Pharmacology, SUNY Upstate Cancer Research Institute, SUNY Upstate Medical University, Syracuse, NY 13210, United States

[b] Department of Obstetrics and Gynecology, Union Hospital, Tongji Medical College, Huazhong University of Science and Technology, Wuhan, HuBei 430022, China

[c] Department of Applied Chemistry, College of Science, China Agricultural University, Beijing 100193, China

[#] These authors contributed equally to this work.

Abstract

Cisplatin (CDDP) and paclitaxel (PTX) are two established chemotherapeutic drugs used in combination for the treatment of many cancers, including ovarian cancer. We have recently developed a three-layered linear-dendritic telodendrimer micelles (TM) by introducing carboxylic acid groups in the adjacent layer via “thio-ene” click chemistry for CDDP complexation and conjugating cholic acids via peptide chemistry in the interior layer of telodendrimer for PTX encapsulation. We hypothesize that the co-delivery of low dosage PTX with CDDP could act synergistically to increase the treatment efficacy and reduce their toxic side effects. This design allowed us to co-deliver PTX and CDDP at various drug ratios to ovarian cancer cells. The *in vitro* cellular assays revealed strongest synergism in anti-tumor effects when delivered at a 1:2 PTX/CDDP loading ratio. Using the SKOV-3 ovarian cancer xenograft mouse model, we demonstrate that our co-encapsulation approach resulted in an efficient tumor-targeted drug delivery, decreased cytotoxic effects and stronger anti-tumor effect, when compared with free drug combination or the single loading TM formulations.

Keywords

Cisplatin; Paclitaxel; Drug delivery; Ovarian cancer; Synergism; Combination chemotherapy

* Corresponding author. Fax: +1 315 464 5143. luoj@upstate.edu (J. Luo)..

Appendix A. Supplementary data

Supplementary data related to this article can be found at http://dx.doi.org/10.1016/j.biomaterials.2014.10.044.

1. Introduction

Combination chemotherapy is a common strategy to treat cancer in the clinic due to the rapid development of drug resistance and heterogeneity of cancer cells. As such, specific guidelines have been implemented to treat various cancers more effectively using a combination of distinct chemotherapeutic drugs. In recent years, cisplatin (CDDP) and paclitaxel (PTX) have been two of the most popular drugs used against various tumors, including ovarian cancers. Per National Comprehensive Cancer Network (NCCN) guidelines, combination chemotherapy with platinum and taxanes is standard of care for primary treatment of ovarian cancer. CDDP binds DNA and inhibits DNA synthesis; while PTX arrests cell cycles via stabilizing microtubules. Given their distinct mechanisms of action, it has been demonstrated that co-administration of CDDP and PTX achieve synergistic effects on cancer cells [1,2]. Interestingly, PTX showed strong synergism when it was administered first; however, it showed antagonistic effects when administered after CDDP in ovarian cancer patients [3,4]. This observation has led to improved combination drug regimens and more effective management of ovarian carcinoma [5]. At the same time, special attention must be paid to the severe side effects of PTX and CDDP combination regiments, e.g. neutropenia, kidney dysfunction, peripheral neuropathy, etc, that can be dose limiting toxicities. Despite the improvements in the modern ovarian cancer treatment via the combination of optimal cytoreductive surgery, platinum-based chemotherapy, and novel targeting strategies [6], ovarian cancer is still rarely curable [5]. Therefore, tolerability of treatment and quality of life remains an important issue.

PTX is about 1000 times more potent than CDDP (IC50s: low n_M *vs* low μM) in a wide variety of cancer cells in culture. However, much higher dose of PTX (175 mg/m^2 every three weeks) could be used for cancer treatment than CDDP (75–100 mg/m^2 every four weeks). It reflects the relative low systemic toxic side effects of PTX at the same dose level than CDDP, due to the fast *in vivo* clearance and metabolism of PTX as an organic molecule compared with the heavy metal drug CDDP [7,8]. On the other hand, the poor pharmacokinetics ($t_{1/2}$ in human: 0.34 h) [8] and pharmacodynamic profiles (cytochrome P450 metabolism) [9,10] of PTX may limit the tumor accumulation and hinder the *in vivo* efficacy of PTX. In contrast, CDDP dominantly binds to serum proteins and is eliminated and metabolized much slower *in vivo* [7,8]. The dissociated CDDP and its metabolites lead to long-term drug exposure of cancer cells, as well as normal tissues. Consequently, CDDP is a highly active anticancer drug, but with significant acute and chronic nephro-, oto-, and peripheral neuro-toxicity [11]. Therefore, an important goal in optimization of PTX/CDDP combination therapy is to increase PTX bioavailability and drug exposure to tumor, while at the same time, decreasing the acute and chronic toxic side effects of CDDP. This could be achieved by modifying the PK/PD profile, tumor uptake and biodistributions of both drug molecules via the nanoparticle-based drug delivery system. Given the high therapeutic index of CDDP *in vivo*, many combinational chemoregimens are based on CDDP to achieve better cancer treatment in clinic. Therefore, it would be efficacious to combine CDDP at an even increased dose level with the reduced toxicity via nano-formulation with a relative low dose of PTX for synergistic cancer treatment, thereby overcoming drug resistance. In addition,

even low dose of PTX could be therapeutic after being efficiently delivered to tumor sites via nanocarriers.

Over the last two decades, nanoparticle-mediated drug delivery systems have been demonstrated to be effective methods for the targeted delivery of chemotherapeutic drugs, while reducing the apparent toxic side effects [12,13]. Various nanocarrier systems have been developed for platinum drug delivery [14]. However, it is challenging to encapsulate two drugs with distinct chemical and physical properties into one nanocarrier, such as hydrophobic PTX and metallic CDDP. Recently, a few studies have been reported on co-delivery of CDDP [15,16], or Platinum prodrug (Pt-IV) [17–20] together with other hydrophobic chemodrugs, such as PTX [15, 20], docetaxel [16,18], daunorubicin [19], and gambogic acid [21], etc, to improve anticancer effects. However, versatile nanocarriers are still needed to fine tune the drug loading ratio and control the drug release profiles to maximize the synergism of PTX and CDDP combination in ovarian cancer treatment.

We have developed a linear-dendritic copolymer system (named as telodendrimer) for efficient hydrophobic anticancer drug delivery, such as PTX [22,23]. Here, we further modify telodendrimer via introducing a segregated domain containing carboxylic functional groups for the co-delivery of CDDP and PTX. We characterize the drug loading properties, biodistribution, toxicities and determine the synergism of combination nanotherapeutics in anti-tumor effects in ovarian cancer mouse models.

2. Material and methods

2.1. Materials and instruments

Paclitaxel was purchased from AK Scientific Inc. (Mountain View, CA). CDDP was purchased from Sigma–Aldrich. DiI was purchased from (AAT, Bioquest). Mono methoxyl terminated poly(ethylene glycol) monoamine (MeO-PEG-NH_2, M.W.: 5000 Da) was purchased from JenKem Technology, USA Inc. (Fmoc)Lys(Boc)-OH, (Boc)Lys(Boc)-OH and (Fmoc)Lys(Fmoc)-OH were purchased from AnaSpec Inc. (San Jose, CA. USA). The MALDI matrix α-Cyano-4-hydroxycinnamic acid was purchased from Sigma Aldrich Chemical Co, used as supplied. Cholic acid and all other chemical reagents were purchased from Sigma–Aldrich. Dialysis membrane with 3500 MW cut off was purchased from Spectrum Laboratories, Inc. The preparations of cholic acid derivatives (Cholic acid NHS ester) were described in the previous publication [22] ^{1}H NMR spectra were recorded on a Bruker AVANCE 600 MHz spectrometer. Mass spectra were acquired using a Bruker REFLEX-III MALDI-TOF mass spectrometer, equipped with a nitrogen laser delivering 3 ns laser pulses at 337 nm. Particle sizes of micelles were measured via a dynamic light scattering (DLS) particle sizer (Zetatrac, Microtrac Inc.) and also observed under a transmission electron microscope (TEM) JEOL JEM-2100 HR instrument at a voltage of 200 kV after staining with uranyl acetate solution. Zeta potential of TM before and after CDDP loading was measured via zetasizer (Malvern Inc.) in pure water.

2.2. Telodendrimer synthesis

The nomenclature of the telodendrimers followed the system used in the previous studies: For example, telodendrimer $PEG^{5K}(COOH)_8$-L-CA_8 indicates that the molecular weight of PEG is 5 kDa and there are 8 carboxyl group conjugated on the adjacent layer; eight cholic acid molecules were conjugated at the distal peripheral of telodendrimer and were segregated with a triethylene glycol linker molecule (L). The telodendrimers were synthesized using a solution-phase condensation reaction starting from MeO-PEG^{5k}-NH_2 (5000 Da) via stepwise peptide chemistry following the previous procedure [22,23], and briefly described as following:

(Fmoc)Lys(Boc)-OH was coupled onto the terminal amino group on PEG by using DIC and HOBt as coupling reagents until a negative Kaiser test result was obtained, which indicated the completion of the coupling reaction. PEGylated molecules were precipitated by pouring reaction solution into excess amounts of cold ether, followed by centrifugation and then washed with cold ether one or two times. The white powder precipitate was then dried under reduced pressure and the Fmoc protection group was removed by using 20% methylpiperidine solution in DMF and then polymer was precipitated. Second coupling of (Fmoc)Lys(Boc)-OH was coupled repeatedly. After removal of Fmoc groups on polymer, Fmoc protected triethylene glycol linker molecule [24] was coupled to the terminal amino groups. Then three consecutive coupling of (Fmoc)Lys(Fmoc)-OH were carried out to generate a dendritic polylysine terminated with eight Fmoc groups and two Boc-protected amino groups at the adjacent sites of polymer. Further, PEG^{5K}-$(NH\text{-}Boc)_4$-$Le(NH–Fmoc)_8$ was obtained via coupling of (Boc) lys(Boc)OH onto the adjacent amino groups of the telodendrimers after removal of two Boc groups with 50% (v/v) trifluoroacetic acid (TFA) in dichloromethane (DCM). Four allylacetic acid were coupled on the amino groups after removal of Boc groups by using HOBt/DIC as coupling reagents to form PEG^{5K}-$(Allyl)_4$-$Le(NH–Fmoc)_8$ (**I**). Cholic acid NHS esters were then coupled to the Fmoc-functionalized amino groups of dendritic polylysine after removal of Fmoc group to yield PEG^{5K}-$(Allyl)_4$-L-CA_8 (**II**). 2-mercaptosuccinic acid molecules were finally coupled to the double bond via thioene click chemistry [25] with the AIBN as initiator in THF under refluxing to generate carboxyl groups containing telodendrimer (**III**) $PEG^{5K}(COOH)_8$-L-CA_8.

The structures of intermediate telodendrimers **I**, **II** and **III** were characterized via ^1H NMR to monitor the yield of each step. The final product was purified via dialysis against pure water for three days. Dialysis media was refreshed every 4 h.

2.3. Drug loading process

CDDP and PTX dual-drug-loaded micelles were prepared via a two-step method. TM aqueous solution was mixed with an aqueous solution of CDDP (1 mg/mL) at a molar ratio of ([cisplatin]/[COOH] = 1:2) and incubated at 37 °C for 48 h. Unbound CDDP was removed by ultrafiltration device (molecular weight cut-off size (MWCO) 5,000Da, Corning). The re-suspended solution was freeze-dried to obtain the CDDP-loaded powder $TM_{(CDDP)}$. Next, $TM_{(CDDP)}$ was dissolved in chloroform and different amount of PTX (CDDP/PTX = 1:1, or 2:1, 4:1, w/w) was added and dissolved into the solution. Organic solvent was evaporated on a rotavap apparatus to obtain a homogeneous dry polymer film

coated on the flask wall. Then it was further dried under high vacuum for 30 min. The thin film was dissolved into 1 mL distilled water, followed by sonication for 5 min, allowing the sample film to disperse into micelle solution. After 5000 rpm centrifuged for 5 min, the supernatant solution was filtered through a 0.45 μm filter to remove the unbound PTX precipitates. Pt content in the micelles was determined on an Inductively Coupled Plasma Optical Emission Spectrometer (ICP-OES, PerkinElmer) calibrated with Pt (2–100 ng/mL) and iridium as the internal standard. PTX levels were determined by high-performance liquid chromatography (HPLC, Shimadzu corporation) analysis. The mobile phase was composed of 55% of acetonitrile in water. The elute time was 10 min, the reverse phase column was a C18 (5 μm, 4.6 × 150 mm). The column temperature was maintained at 30 °C. The flow rate was set at 1.0 mL/min and the detection wavelength was 227 nm. Docetaxel was used as an internal reference in HPLC analysis. The drug loading content (DLC%) and drug loading efficiency (DLE%) were calculated following the formula below:

$$DLC\% = (\text{mass of drug in micelles}/\text{mass of drug loaded micelles}) \times 100\%$$
$$DLE\% = (\text{mass of drug in micelles}/\text{total mass of drug for loading}) \times 100\%$$

2.4. Drug release and micellar stability

Drug release from dual-drug-loaded micelles was examined in saline by dialysis method using a dialysis cartridge (Pierce Chemical Inc) with a 3.5 KDa MWCO. The dialysis was kept at 37 °C and swirled at 100 rpm. The concentrations of PTX and Pt(II) remained in the dialysis cartridge at various time points was measured by HPLC and inductively coupled plasma mass spectrometry (ICP-MS, PerkinElmer), respectively.

2.5. Critical micellization concentration (CMC)

A series concentrations of empty TM, TM $_{(CDDP)}$, TM $_{(PTX)}$ and TM $_{(CDDP/PTX)}$ solutions in 0.01 M PBS were prepared in the range from 0.4 to 200 mg/mL Nile Red solution (20 μM) in MeOH was added to a series of wells of a 96-well plate. After MeOH was evaporated under vacuum, 100 μL of TM solutions at different concentrations were added to each well to obtain a final concentration of 1 μM Nile Red and mildly shaken overnight in dark at room temperature. Then, the fluorescent emission was measured at the wavelength of 620 nm (excited at 543 nm) using a micro-plate reader (BioTek, USA), and plotted vs the concentration of the telodendrimers. The CMC was determined by the threshold concentration, where the fluorescent intensity increases markedly.

2.6. Hemolytic assays

One mL of fresh blood from healthy human volunteers was collected into 10 mL of PBS solution in the presence of 1.5 mg/mL 20 mM EDTA. Red blood cells (RBCs) were then separated by centrifugation at 1000 × g for 10 min. The RBCs were then washed three times with 10 mL of PBS, and re-suspended in 20 mL PBS. 200 μL of diluted RBC suspension was mixed with polymers at serial concentrations (10, 100, 500 and 1000 μg/ mL) by gentle vortexing and incubated at 37 °C. After 0.5 h, 4 h and overnight, the mixtures were centrifuged at 1000 × g for 3 min. The supernatant free of hemoglobin was determined by measuring the UV absorbance at 540 nm using a UVevis spectrometer (Thermo scientific).

Incubations of RBCs with Triton-100 (2%) and PBS were used as the positive and negative controls, respectively. Triton X-100 (10 g/L) is a surfactant known to lyse RBCs. The hemolysis ratio of RBCs was calculated using the following formula: Hemolysis% = $(OD_{sample} - OD_{PBS})/(OD_{triton} - OD_{PBS}) \times 100\%$. All hemolysis experiments were carried out in triplicates.

2.7. Confocal fluorescence cell imaging

The cellular uptake and intracellular trafficking of TM nanoparticles were determined via confocal laser scanning microscopy. DiI (a hydrophobic cyanine dye) was encapsulated together with CDDP into the TM to probe the nanoparticles in cell. SKOV-3 cells were seeded in chamber slide with a density of 5×10^4 cells per well in 350 μL of McCoy's 5A and cultured for 24 h. And then original medium was replaced with free DiI and DiI-loaded $TM_{(DiI\text{-}CDDP)}$ at the final DiI concentration of 1 mg/mL at 37 °C or 4 °C, respectively. After 30 min or 2 h incubation, the cells were washed three times with cold PBS and fixed with 4% formaldehyde for 10 min at room temperature, and the cell nuclei were stained with DAPI. The slides were mounted with cover slips and cells were imaged with a NiKON FV1000 laser scanning confocal fluorescence microscopy.

2.8. In vitro synergistic cytotoxicity

The cytotoxicity of blank micelles and drug-loaded micelle were assessed by measuring the cell viability using the standard MTS assay. SKOV-3 ovarian cancer cells and ES-2 ovarian cancer cells were seeded in 96-well plates at 4×10^3 cells per well in 100 μL of McCoy's 5A with L-glutamine containing 10% fetal bovine serum, supplemented with 50 U/mL penicillin and 50 U/mL streptomycin, and incubated at 37 °C in 5% CO_2 atmosphere for 24 h. Different concentrations of the empty micelle solutions and drug-loaded micelles were added into the cell medium. After 72 h incubation, Cell Titer 96® Aqueous Cell Proliferation Reagent, which is composed of MTS and an electron coupling reagent PMS, was added to each well according to the manufacturer's instructions. The cell viability was determined by measuring the absorbance at 490 nm using a micro-plate reader. The wells contained untreated cells served as blank controls. Results were shown as the average cell viability $[(OD_{treat} - OD_{blank})/(OD_{control} - OD_{blank})\ 100\%]$ of triplicate wells.

The effective method to evaluate synergistic drug combinations *in vitro* is median-effect analysis, as originally proposed by Chou and Talalay [26,27]. The median-effect method assesses the drug–drug interaction by a term called the “combination index” (CI), which is based on the concentrationeresponse relationship. CI was used to evaluate synergy between CDDP and PTX combination against SKOV-3, ES-2, and Hela cells *in vitro*. Values of CI < 1, CI = 1, and CI > 1 indicate synergy, additivity, and antagonism, respectively. CI analysis was performed by CalcuSyn software 1.0.

2.9. Xenograft mouse models

Female athymic nude mice (Nu/Nu strain), 5–6 weeks age, were purchased from Harlan (Livermore, CA). All animals were kept under pathogen-free conditions according to AAALAC (Association for Assessment and Accreditation of Laboratory Animal Care) guidelines and were allowed to acclimatize for at least 4 days prior to any experiments. All

animal experiments were performed in compliance with institutional guidelines and according to protocol approved by the Animal Use and Care Administrative Advisory Committee. SKOV-3 ovarian cancer cells (7×10^6) in a 100 μL of mixture of PBS and Matrigel (1:1 v/v) without fetal bovine serum (FBS) were injected subcutaneously into the flanks of nude mice to form nodules.

2.10. Optical animal imaging

Nude mice bearing human SKOV3 ovarian cancer tumor (approximately 500 mm^3) were randomized into 2 groups (3 mice per group). DiD (a hydro-phobic near-infrared (NIR) cyanine dye) was encapsulated in each nanocarrier (together with PTX and CDDP) at a ratio of 2:1:0.1 (CDDP/PTX/DiD by weight) using the same method as described above. The particle size was measured by DLS analysis. 100 μL of $TM_{(DiD\text{-}PTX\text{-}CDDP)}$ solution was filtered with a 0.22 μm filter to sterilize solution before injection. At the same time, same amount of DiD in DMSO solution was diluted with PBS right before I.V. injection. The fluorescent DiD co-loaded TM with equivalent dose of 6 mg/kg CDDP were injected into nude mice bearing SKOV-3 tumor xenograft via tail vein. Mice were anesthetized via isoflurane and optically imaged at different time points (1 h, 2 h, 4 h, 8 h, 24 h, 48 h and 72 h) using an IVIS 200 (PerkinElmer) with the (excitation/ emission 625/700 nm). At the end of the experiments, the animals were sacri-ficed and all the major organs as well as tumors were excised for *ex vivo* imaging to determine the *in vivo* biodistribution of nanoparticles. The associated fluorescence intensities were determined by Living Image software (Caliper Life Sciences) using operator-defined regions of interest (ROI) measurements.

2.11. Phamocokinetics and biodistribution

The blood pharmacokinetics study were performed using female SPF BALB/c mice, which were purchased from Charles River Laboratories Inc. Nanocarriers were administered into mice via tail vein injection with free drug mixture of CDDP/PTX or co-loading TM (CDDP/PTX = 2:1) solution at a single equivalent dose of CDDP/PTX 6/3 mg/kg via tail vein. At defined time points (5 min, 0.5 h, 1 h, 2 h, 4 h, 8 h, 24 h and 48 h), blood samples were collected into heparinized tubes and immediately centrifuged at 1000 rpm for 15 min to obtain plasma. Plasma samples were dissolved on heat in nitric acid and the platinum contents were measured by ICP-MS. The percentage of injected dose in plasma was calculated considering plasma volume in mice to be 45.6 mL/kg [28].

In another set of the experiments, nude mice bearing human SKOV3 ovarian cancer tumor (approximately 500 mm^3) were randomized into 2 groups (3 mice per group). Free CDDP and TM (CDDP/PTX = 2:1) were injected into nude mice via tail vein at a single equivalent dose of CDDP 6 mg/kg. At 48 h post-injection, major organs (heart, liver, spleen, lung and kidney) and tumor tissues were harvested from the mice. The organs were weighed and dissolved in the concentrated nitric acid by heating up (70 °C) and evaporated to dryness, and then re-dissolved in 0.1 N HCl for tissue biodistribution of Pt analysis by ICP-MS.

2.12. Evaluation of the acute toxicity

Six-week-old female SPF BALB/c mice were randomized based on body weight into 3 groups ($n = 3$). Mice were administered PBS, free drug mixture of CDDP/PTX = 2:1 or TM

(CDDP/PTX = 2:1) at a single equivalent CDDP dose of 10 mg/kg through tail vein injection. The physical states and body weight change of the mice were monitored every day. On day 7 after injection, the blood was collected into heparinized tubes through cardiac puncture under anesthesia and animals were euthanized via CO_2 overdose and kidneys and livers were harvested and imbedded in OCT (Optimal Cutting Temperature Compound, Sakura Finetek USA, Inc) and stored at −80 °C for further analysis. Serum were isolated and the clinical chemical parameters, including alanine aminotransferase (ALT), aspartate aminotransferase (AST) and blood urea nitrogen (BUN) were analyzed at the Cornell University Animal health Diagnostic Center. In addition, WBC, RBC and platelet were counted. Livers and kidneys were cut into serial 5 μm sections and fixed with 4% paraformaldehyde and stained with hematoxylin and eosin (H&E) for pathology analysis.

2.13. Evaluation of toxicity during the repeated treatment

Six-week-old female SPF BALB/c mice were administered intravenously 3 times at 4-day intervals with free drug mixture (CDDP/PTX = 2:1) or TM $_{(CDDP/PTX = 2:1)}$ at the doses of CDDP 4 or 6 mg/kg body weight, respectively. The physical conditions and body weight change of mice were monitored daily for four weeks. On day 7 after last injection, the blood was collected from each mouse for blood cell counting analysis. The MTD was defined as the allowance of a median body weight loss of 15% and causing neither death due to toxic effects nor remarkable changes in the general signs within two weeks after administration.

2.14. In vivo anticancer efficacy

Nude mice bearing human SKOV3 ovarian cancer tumor (approximately 150 mm^3) were randomly divided into 6 groups (n = 5), including control (PBS only), free CDDP (4 mg/kg CDDP), TM $_{(PTX)}$ (3 mg/kg PTX), PEG$_{(CDDP)}$ (4 mg/kg CDDP), TM $_{(CDDP)}$ (6 mg/kg CDDP), and TM $_{(CDDP/PTX = 2:1)}$ (6 mg/kg CDDP, 3 mg/kg PTX). Treatments were administered 3 times totally via tail vein on day 0, 4 and 8. Animal body weight and tumor volume were monitored every second day. Seven days after the last treatment, about 100 μL of blood was collected via tail bleeding for blood counts. The tumor sizes were measured with electronic calipers, and calculated using the following formula: V = (shortest diameter^2 × longest diameter)/2. Animal were sacrificed when tumor volume exceeded 1500 mm^3, or the greatest tumor dimension exceeded 20 mm, or tumor became necrotic, or animal exhibited a body weight loss of more than 20%.

2.15. Statistical analysis

The level of significance in all statistical analyses was set at a probability of $p < 0.05$. Data are presented as means ± standard error (SEM). Statistical analysis was performed by Student's t-test for comparison of two groups, and one-way analysis of variance (ANOVA) for multiple groups, followed by Newman-Keul's test if overall $p < 0.05$.

3. Results and discussion

In our previous studies, we have developed a linear PEG-block-dendritic oligo-cholic acid named as telodendrimer, which severed as an efficient micelle nanocarrier for delivering hydrophobic drugs, e.g. PTX. The telodendrimers are synthesized via a well-controlled

peptide chemistry, which allows us to engineer the architecture and functionality of the telodendrimer nanoparticle to enhance the delivery of anticancer drugs. In this study, we introduced multiple carboxyl groups onto an adjacent site of telodendrimer using peptide chemistry and the thio-ene click chemistry (Scheme 1). The resulting telodendrimer enables both the loading of platinum drugs via carboxyl chelating and the encapsulation of hydrophobic molecules like paclitaxel in the interior core of the micelles.

3.1. Telodendrimer synthesis and characterization

Following the procedure in our previous publication [22], telodendrimers were synthesized from amino group of MeO-PEG^{5k}-NH_2 via solution phase peptide chemistry (Scheme S1). Kasier tests were performed during each step of peptide coupling reactions to ensure the completion of the reaction [29]. Furthermore, ^{1}H NMR was used to characterize the chemical structures of the intermediate and the final telodendrimer. The chemical structure of the important intermediates, i.e. PEG^{5k}$(Boc)_2$-L-$(Fmoc)_8$ and PEG^{5k}$(-Boc)_4$-L-$(Fmoc)_8$ was confirmed via MALDI ToF MS (Supporting information Fig. S2) and 1H NMR analysis with the doubling signal of Boc groups observed (Supporting information Fig. S1 and S3). Further, four allylacetic acid molecules were coupled on the amino groups by using HOBt/DIC as coupling reagents after the removal of Boc groups to form PEG^{5K}-$(Allyl)_4$-L–$(NH–Fmoc)_8$ (**I**). Cholic acid NHS esters were then coupled on the peripheral of dendritic polylysine after removal of Fmoc groups to yield PEG^{5K}-$(Allyl)_4$-L-CA_8 (**II**). Subsequently, 2-mercaptosuccinic acid molecules were added to the vinyl double bond via “thio-ene” click chemistry to introduce carboxyl groups onto telodendrimer (**III**) PEG^{5K}$(COOH)_8$-L-CA_8 [30].

As shown in Fig. 1, signature peaks for vinyl protons (5.7 ppm and 4.8–5.0 ppm) were evident within the telodendrimer with detected number close to the theoretical number of 4 based on the area integration relative to the methyl signal on MeO-PEG (3.2 ppm). In addition, protons of the Fmoc protecting groups were shown at 7.2–7.8 ppm and 4.0–4.4 ppm. After removal of Fmoc and CA conjugation, three unique methyl groups of CA appeared from 0.5 to 1 ppm and some other signature protons of CA, e.g. –OH and –OCH–, were shown between 3.6 and 4.3 ppm in NMR spectrum of telodendrimer II. After the last step of thio-ene click chemistry, carboxylic acids were detected in telodendrimer III at 12.5 ppm. MALDI-ToF MS spectrophotometer and NMR analysis revealed the composition of the final telodendrimer III to be PEG^{5k}$COOH_{6.3}$-L-$CA_{6.2}$ and an approximate molecular weight of 9470 Da (Fig. 2 and Table 1). The telodendrimer III self-assembles into micelles. The critical micellization concentration (CMC) of the micelles were measured to be 29.6 μg/mL using Nile Red as a fluorescent probe. The zeta potential of the empty telodendrimer micelles (TM) was measured to be −11.3 mV in pure water, which was shifted to 3.1 mV after CDDP complexation (Fig. 2).

The empty telodendrimer micelle has a hydrodynamic diameter of 9.0 ± 2.6 nm determined by dynamic light scattering (DLS) particle sizer. This size is smaller than the typical telodendrimer PEG^{5k}CA_8 (~20 nm), due to the decoration of the hydrophilic carboxyl groups. It will be feasible to first encapsulate PTX physically into the hydrophobic core of micelle, then incubated with CDDP in aqueous solution for CDDP loading. However, it was

found that the single loading of PTX had poor reproducibility and was sensitive to pH. The loading of PTX in acidic solution (pH 4–5) could yield stable micelles with monodispersed particle sizes (16.0 ± 3.7 nm) at a 10:1 polymer/drug mass ratio. However, the particle sizes of the PTX-loaded micelles $TM_{(PTX)}$ increase and become heterogeneous with the increase of pH at neutral or basic condition, which is preferred for CDDP complexation. This is due to the charge repulsion of the deprotonated carboxyl groups in telodendrimer, which destabilize the micelles and the payload drug molecules. Therefore, an alternative approach was adopted to load CDDP first in pure water and then encapsulate PTX. The rational is that the CDDP complexation could neutralize carboxyl groups and restore the balanced amphiphilicity of telodendrimer for efficient PTX loading. The particle sizes of TM with single CDDP loaded were detected via DLS to be 16.9 ± 3.7 nm (Supporting information Fig. S5). The drug loading content (DLC) and drug loading efficiency (DLE) were measured via ICP-OES to be 10% and 97%, respectively. After lyophilization, $TM_{(CDDP)}$ powder was used for PTX loading via a thin-film dispersion method. The CMCs of drug-loaded micelles were decreased slightly to 26.8 and 23.8 μg/mL after single loading of CDDP and the coloading of CDDP/PTX (2:1 by weight), respectively (Supporting information Fig. S6).

After co-loading of CDDP and PTX at a ratio of polymer/PTX/ CDDP at 5:0.5:0.2 mg/mL, the particle had a similar sizes of 16.9 ± 4.8 nm (Fig. 3), where the PTX loading efficiency was detected to be 92% by HPLC. When the particles contained CDDP/ PTX at different ratios, e.g. $TM_{(CDDP/PTX = 1:1)}$, $TM_{(CDDP/PTX = 2:1)}$, $TM_{(CDDP/PTX = 3:1)}$ and $TM_{(CDDP/PTX = 4:1)}$, the apparent diameters were similar around 20 nm by DLS. TEM images revealed that majority of empty and drug-loaded micelles had similar spherical shape that increased slightly in size between 10 and 20 nm with the addition of the chemotherapeutic drug (Fig. 3). We noticed a few worm-shaped micelles in TEM image; It was likely formed *in situ* during surface deposition in TEM sample preparation, which was absent in subsequent cryo-TEM analysis (Fig. 4A).

3.2. Drug release and stability of $TM_{(CDDP/PTX)}$ in vitro

The assembled nanoparticles were assessed to be highly stable after prolonged incubation, e.g. storage at 4 °C for a month (Fig. 4A). In addition, the cryo-TEM imaging revealed the homogenous particle sizes of $TM_{(CDDP/PTX)}$ over storage (Fig. 4A). The drug release profiles for both PTX and CDDP from $TM_{(CDDP/PTX)}$ were studied via a dialysis experiment against saline. As shown in Fig. 4B, PTX released much faster (50% release within 24 h) than CDDP (50% release within 92 h). To determine the blood compatibility of nanotherapeutics, we incubated the empty and drug assembled nanoparticles with human red blood cells *in vitro*. None hemolytic activity was observed from both the empty TM and drug-loaded TMs (Supporting information Fig. S7) even at a high polymer concentration of 1 mg/mL after overnight incubation.

3.3. Cellular uptake

In order to visualize and determine the overall intracellular trafficking of TMs, we incorporated a fluorescent dye (DiI) into micelles loaded with CDDP and PTX, which was incubated with SKOV-3 ovarian cancer cells for confocal cell imaging. The amphiphilic dye DiI has been demonstrated to be a stable probe molecule to trap the intracellular trafficking

of polymer micelles [31]. As shown in Fig. 5, free DiI quickly diffused into the mammalian cells, which was strongly hindered when the dye was embedded into the nanoparticles. It was observed that temperature has less impact on the free DiI diffusion. In contrast, the cell uptake of $TM_{(DiI/CDDP/PTX)}$ was almost depleted at 4 °C, which indicates the energy dependent process for nanoparticle uptake (Fig. 5A and Supporting information Fig. S8). In addition, the cells were also stained with lysotracker green to label lysosome within cytoplasm. Here, we found that cells treated with the TM nanoparticle formulations had stronger co-localization of DiI dye within the lysosome compartments (Fig. 5B), indicating the endocytosis pathway for TM to deliver its contents into cells.

3.4. In vitro synergistic cytotoxicity

It has been reported that the synergistic combinations of CDDP and PTX depends largely on the dosing sequence, time interval and dose concentrations of these two drugs [32]. Given the nature of our nanoparticle, it is likely that the faster PTX release kinetics favor a pattern that is consistent with current anticancer combinatorial regiments (Fig. 4). The empty TM showed non-cytotoxic up to 1 mg/ mL concentration after 72 h incubation with several cell lines, including SKOV3 ovarian cancer cells (Supporting information Fig. S9). The single loading of either CDDP or PTX exhibited slightly reduced potency compared with the free drugs against SKOV3 cells because of slow drug release profiles (Fig. 6). After co-loaded with different ratio of CDDP and PTX, the cytotoxicity of the $TM_{(CDDP/PTX)}$ were significantly increased in killing ovarian cancer cells, compared with free CDDP, due to the high potency of PTX (Fig. 6A). Importantly, the IC_{50}s of PTX were also further decreased upon of the addition of CDDP, which show nontoxic at this concentration (IC50s: CDDP: 1354 ng/mL; PTX: 32 ng/mL, shown in Table 2). It was interesting to observe the best cell killing at the combination of 2:1 ratio of CDDP/PTX in the co-loading formulations with the lowest combination index of 0.21 at 50% of cell killing (CI50) on SKOV-3 cells, which have higher IC50s to CDDP (1354 ng/ mL) and $TM_{(CDDP)}$ (3172 ng/mL) than ES2 cells (920 and 1429 ng/mL, respectively), indicating a strong synergism on resistant SKOV-3 cells [33,34]. According to the definition of CI, values of $CI < 1$, $CI = 1$, and $CI > 1$ indicate synergy, additivity, and antagonism, respectively. As shown in Table 2, the similar trends in cell growth inhibition via the combination therapy were observed in ES2 and Hela cells (Supporting information Fig. S10).

Furthermore, the CIs of the whole cell killing panel were analyzed via CalcuSyn software. It clearly demonstrated the synergism for $TM_{(CDDP/PTX = 2:1)}$ in almost the whole range of Fa with $CI < 1$ in all three cell lines. (Fig. 6C, D&E). However, for $TM_{(CDDP/ PTX = 4:1)}$, CI value declined gradually along with the rise of Fa, but it was more than 1 when Fa was at the range of 0.05–0.4. Regarding to $TM_{(CDDP/PTX = 1:1)}$, CI increases gradually along with the rise of Fa, and exceeds $CI = 1$ in the Fa range of 0.4–0.95. The similar trend of synergism of $TM_{(CDDP/PTX)}$ were observed in ES2 cells and Hela cells. $TM_{(CDDP/PTX = 2:1)}$ exhibited the best cancer cell killing effects (lowest IC50) via synergistic drug combination in all three cell lines.

3.5. Fluorescence animal imaging

Non-invasive and real time near-infrared fluorescence (NIRF) imaging was utilized to image the tissue distribution and tumor accumulation of nanocarriers *in vivo*. To track the *in vivo* fate of the TM nanocarriers and probe the biodistribution of the hydrophobic PTX in the nanocarriers, a NIRF hydrophobic dye DiD was encapsulated together with CDDP and PTX at 2:1 ratio (w/w) into TM nanocarriers as determined previously. The particle sizes were measured to be 20.4 ± 3.8 nm via DLS (Supporting information Fig. S11). The *in vivo* fluorescent optical imaging of whole body (Fig. 7A) showed that DiD-labeled $TM_{(CDDP/PTX)}$ micelles were able to gradually accumulate at the SKOV-3 tumor xenograft starting at 2 h and reached a plateau at 24 h and throughout the 72 h period after tail vein injection (Fig. 7B). In contrast, very weak tumor fluorescence was observed in the mice injected with free DiD. At 72 h of post-injection, tumor and other major organs were harvested for *ex vivo* NIRF imaging to compare the tissue distribution of TMs (Fig. 7C). As shown in Fig. 7D, DiD-loaded $TM_{(CDDP/PTX)}$ micelles were mainly accumulated in tumor with more than 4-fold higher intensity than that in the vital organs, e.g. liver, lung, spleen and kidney. While, DiD was mainly taken up by spleen and liver in the mice treated with the free DiD, whereas low intensity in tumor. It may be resulted from the aggregation of highly hydro-phobic DiD in free DiD administration.

3.6. Pharmacokinetics and biodistribution of $TM_{(CDDP/PTX)}$ in vivo

CDDP concentrations were analyzed in the following pharmacokinetic (PK)-biodistribution study. The PK profile of Pt in plasma were analyzed via the HCP-MS at defined time points after intravenous administration of free drug mixtures CDDP/PTX or $TM_{(CDDP/PTX)}$ nanoformulation in nude mice (Fig. 8A). The maximum detected Pt concentrations in plasma at 5 min was approximately 3 times greater for the nanoformulation over free drug injection (88 μg/mL and 27.6 μg/mL respectively). Free CDDP was rapidly cleared from plasma, and only 5% Pt of injected dose was detected in plasma at 30 min after injection and less than 1% at 24 h post-injection. Markedly, the $TM_{(CDDP/PTX)}$ nanocarrier displayed slower clearance rates, with approximately 75% and 13% of total Pt remained at 30 min and 24 h, respectively.

The pharmacokinetic parameters were calculated using a two compartment model with PKsolver [35]. As shown in Table 3, the half life time of $TM_{(CDDP/PTX)}$ were increased by 16-fold and 3-fold for α-phase and β-phase elimination, respectively, compared with free CDDP administration. The clearance rate (Cl) of free CDDP were analyzed to be much higher (20–25 fold) than nanotherapeutics for both phases. In addition, the area under the curve (AUC) for the mice treated with $TM_{(CDDP/PTX)}$ was calculated to be 627.44 *vs* 30.8 μg/ml*h for the free CDDP injection. Furthermore, the steady-state volume of distribution (V_{ss}) of Pt was effectively decreased by more than 20-fold in the nanoformulation over free CDDP drug, indicating that the nanoparticle was more effective at retaining CDDP in the systemic circulation. These results strongly suggest that our nanoparticle has a long-circulating half life and is stable within the systemic circulation.

NIRF optical imaging (Fig. 7) has indicated the preferred tumor uptake of the TM and the hydrophobic payload. Further, the tissue biodistribution of Pt were measured via HCP-MS at

the end of PK studies at 48 h post-injection. As shown in Fig. 8B, TM formulations significantly altered the biodistribution and tumor uptake of Pt in animals. In mice treated with TM $_{(CDDP/PTX)}$, the Pt uptakes in the tumor and blood were 4-fold and 5-fold higher than those treated with the free CDDP, respectively ($p < 0.01$). In addition, it was also noted that the accumulation of Pt in kidneys were significantly reduced in the TM $_{(CDDP/PTX)}$ group compared with the group treated with free drug mixture, which may mitigate the Pt-associated nephrotoxicity [36]. Both NIRF imaging and Ptbiodistribution studies indicated the highest tumor uptake of both hydrophobic DiD (as a surrogate of PTX) and CDDP in the animals treated with nanoformulation.

Overall, kidney/tumor and liver/tumor ratio of Pt concentrations were observed to be 4 and 2 respectively in the animals treated with free CDDP. In contrast, in TM$_{(CDDP/PTX)}$ group, Pt concentration in tumor was the highest among all other organs. The comparison of increased tumor uptake and decreased kidney uptake would suggest the increased efficacy and the reduced renal toxicity of TM $_{(CDDP/PTX)}$ nanoformulation. At the same time, Pt concentrations in liver and spleen in mice treated with TM $_{(CDDP/PTX)}$ formulation were 2–5 fold as higher as that in the free CDDP group, which was due to the sustained blood circulation of nanoformulation. Therefore, the toxicity studies need to be done carefully in evaluating liver and kidney functions before and during the combination therapy.

3.7. In vivo toxicity of combination therapeutics

According to the literature, the maximum tolerated dose (MTD) of free CDDP and some other nanoformulations of CDDP were set at 4 mg/kg or lower for cancer treatment in mouse models [37,38]. Therefore, we started testing TM $_{(CDDP/PTX = 2:1)}$ in BALB/c mice at 4 mg/kg of CDDP dosage and escalated the dose with a 50% increment, i.e. 6 mg/kg via tail vein injection for 3 times every four days. There was no obvious body weight loss in 4 mg/kg cohort. And only a mild body weight loss about 7.6% was observed at the dose level of 6 mg/kg on day 10, which were recovered at the end of week 3 (Fig. 9A). No other toxicity signs and animal death was observed in the both groups. Blood cell counting analysis on day 7 after the last injection was conducted and normal cells counting were observed for red blood cell, white blood cells and platelet for both groups (Fig. 9D–E). In this study, the MTD of three-dosage was determined to be higher as CDDP 6 mg/kg/PTX 3 mg/kg for TM $_{(CDDP/PTX = 2:1)}$ in the non-tumor bearing female BALB/c mice.

Acute toxicity of CDDP was studied in BALB/c mice after a single intravenous tail vein injection of the free drug combination (CDDP/ PTX 2:1 w/w) and the combination nanotherapeutics TM (CDDP/PTX = 2:1) at a much higher dosage level of 10 mg CDDP and 5 mg PTX/kg. As shown in Fig. 9B, the mice treated with a free drug mixtures led to about 24 ± 2.14% body weight loss on day 6. In contrast, the TM$_{(CDDP/PTX = 2:1)}$ administration group showed only a small reduction (~2%) in body weight ($p<0.01$). The overall behaviors of mice had no different in TM $_{(CDDP/PTX = 2:1)}$ group compared with the mice in the control group; but the mice treated with high dose of free drug mixture were significantly weaker and less active.

Furthermore, complete blood counting analysis on day 7 revealed decreased amounts of platelets among mice treated with free drug mixtures (CDDP/PTX) compared with the

control group or $TM_{(CDDP/PTX = 2:1)}$ group ($p<0.05$) (Fig. 9D–F). Furthermore, administration of free drug mixture resulted in a significant increase of plasma blood urea nitrogen (BUN), aspartate amino-transferase (AST), and alanine aminotransferase (ALT). However, these values were much lower in mice treated with $TM_{(CDDP/PTX = 2:1)}$ (Fig. 9C), indicating the lower hepatotoxic and renal effects for micellar formulation. The free drug combination of CDDP/PTX at such high dosage of 10 mg/kg significantly increased the BUN level compared with control group and $TM_{(CDDP/PTX = 2:1)}$ group ($p<0.05$), whereas no significant difference was observed between the later two groups. It indicates the relatively low renal dysfunction in animals treated with $TM_{(CDDP/PTX = 2:1)}$. Furthermore, microscopic analysis of the liver and renal parenchyma showed that both organs did not have any morphological changes after the treatment with $TM_{(CDDP/PTX = 2:1)}$, compared with control group (Fig. 10). However, the tubular dilation with flattening of the epithelium cells were observed in the kidneys from the animal treated with free drug mixtures (Fig. 10). Together, these results indicate that the nano-particle enhances the circulation of the drug and reduces the cytotoxic effects on vital organs.

3.8. In vivo anticancer efficacy

To test the efficacy of our design, we delivered various nano-particle formulations to ovarian cancer SKOV-3 xenografted nude mice. Animals were randomly separated into six groups ($n = 5$) and treated with single or combination therapeutics, e.g. free CDDP (4 mg/kg CDDP), TM*(PTX)* (3 mg/kg), PEG(CDDP) (4 mg/kg), $TM_{(CDDP)}$ (6 mg/kg), and $TM_{(CDDP/PTX\ 2:1)}$ (6 mg/kg CDDP & 3 mg/kg PTX), as well as PBS control. Three dosages of drugs and PBS were administered intravenously on day 0, 4, and 8, respectively. The tumor growth inhibitions and body weight changes, survival rates of SKOV-3 tumor bearing mice in different groups were monitored for more than 45 days (Fig. 11). Except free CDDP group, all the mice in the treatment groups tolerated the treatment well with an initial body weight loss less than 10%, followed by the recovery of body weight after day 16 Fig. 11B. However, the body weight loss of mice in the free CDDP treatment group (4 mg/kg) exceeded 20% on day 12 and mouse died due to the toxicity of free CDDP treatment. On day 7 after the last injection, blood samples were collected for blood cell counting analysis. Compared to PBS control group, the WBC counting in free CDDP group was significantly decreased ($p < 0.05$), indicating myelosupression. Whereas, the RBC and PLT in all treatment groups were observed within the normal range (Supporting information Fig. S12).

Unfortunately, all animals in the free CDDP group at 4 mg/kg died on day 12, 13, 15, 16 and 17, respectively, due to the severe side effects as observed in Fig. 11. Low dose TM*(PTX)* (3 mg PTX/kg) showed mild tumor inhibitory effects compared with the control group. At the same time, CDDP loaded in TM exhibited a dose dependent tumor inhibition, which was significantly better than $TM_{(PTX)}$ treatment even at a low dose of 4 mg CDDP/kg. More importantly, $TM_{(CDDP/PTX = 2:1)}$ (6 mg/kg CDDP/3 mg/kg PTX) exhibited better tumor growth inhibition ($p < 0.05$) than $TM_{(CDDP)}$ (6 mg/kg CDDP). On day 28, the median relative tumor volume (RTV) was 2.5 for mice treated with $TM_{(CDDP/PTX = 2:1)}$, while the RTVs for mice treated with $TM_{(CDDP)}$ (4 mg/kg CDDP) and $TM_{(CDDP)}$ (6 mg/kg CDDP) were 11.4 and 5.2, respectively. Superior tumor inhibition of $TM_{(CDDP/PTX = 2:1)}$ could be due to the synergism effect between CDDP and PTX as studied *in vitro*. For humane

reasons, animals were euthanized when the implanted tumor volume reached 2000 mm^3, which was considered as the end point of survival data. The mice survival rates in each group are presented by the Kaplan–Meier survival curve, respectively (Fig. 11C). In general, compared to PBS control, all the CDDP loaded formulations significantly prolonged the survival times of tumor bearing mice. The medium survival time for animals treated with PBS, CDDP (4 mg/kg), $TM_{(PTX)}$ (3 mg/kg), $TM_{(CDDP)}$ (4 mg/kg), $TM_{(CDDP)}$ (6 mg/kg) and $TM_{(CDDP/PTX)}$ (6 mg CDDP + 3 mg PTX/kg) were 19, 15, 23, 27, 34 and 40 days, respectively. The nano-combination cohort $TM_{(CDDP/PTX = 2:1)}$ exhibited longest survival time than all other groups.

4. Conclusion

In this study, we have engineered a three-layered telodendrimer (linear-dendritic polymer) nanocarrier for the effective co-delivery of CDDP and PTX for the ovarian cancer combination therapy. The programmed faster release of PTX than CDDP from the nano-formulation with the optimized drug loading ratio enables the synergism in killing ovarian cancer cells *in vitro*. The stable nano-carrier significantly prolonged the drug delivery in the systemic circulation and reduced the renal toxicity of CDDP. The optical imaging and Pt-biodistribution analysis indicated that telodendrimer micelles were concentrated within tumor sites favorably than in the normal organs. The targeted drug delivery, the increased tolerated dosage and the synergistic combination of CDDP/PTX within telodendrimer nanocarrier enhanced survival of mice harboring ovarian cancers.

Supplementary Material

Refer to Web version on PubMed Central for supplementary material.

Acknowledgment

We greatly acknowledge Prof. Stephan Wilkens for assistance in TEM analysis and Prof. Golam Mohi for the help in blood cell analysis. We thank Dr. Rinki Argawal for helpful discussion. We thank Dr. H. Hans Salamanca for proof reading the manuscript. The financial supports from NIH/NCI R01CA140449 (Luo), Carol M. Baldwin Breast Cancer Research Foundation (Luo) and the institutional startup funds are acknowledged.

References

1. Rowinsky EK, Gilbert MR, McGuire WP, Noe DA, Grochow LB, Forastiere AA, et al. Sequences of taxol and cisplatin: a phase I and pharmacologic study. J Clin Oncol. 1991; 9:1692–703. [PubMed: 1678780]
2. Rowinsky EK, Citardi MJ, Noe DA, Donehower RC. Sequence-dependent cytotoxic effects due to combinations of cisplatin and the antimicrotubule agents taxol and vincristine. J Cancer Res Clin Oncol. 1993; 119:727–33. [PubMed: 8104946]
3. Milross CG, Peters LJ, Hunter NR, Mason KA, Milas L. Sequence-dependent antitumor activity of paclitaxel (taxol) and cisplatin in vivo. Int J Cancer. 1995; 62:599–604. [PubMed: 7665232]
4. Sacchi A, Gasparri A, Gallo-Stampino C, Toma S, Curnis F, Corti A. Synergistic antitumor activity of cisplatin, paclitaxel, and gemcitabine with tumor vasculature-targeted tumor necrosis factor-alpha. Clin Cancer Res. 2006; 12:175–82. [PubMed: 16397040]
5. Coleman RL, Monk BJ, Sood AK, Herzog TJ. Latest research and treatment of advanced-stage epithelial ovarian cancer. Nat Rev Clin Oncol. 2013; 10:211–24. [PubMed: 23381004]

6. Banerjee S, Kaye SB. New strategies in the treatment of ovarian cancer: current clinical perspectives and future potential. Clin Cancer Res. 2013; 19:961–8. [PubMed: 23307860]
7. Undevia SD, Gomez-Abuin G, Ratain MJ. Pharmacokinetic variability of anti-cancer agents. Nat Rev Cancer. 2005; 5:447–58. [PubMed: 15928675]
8. Atta H, Beijnen JH, Vermorken JB, Schellens JHM. Pharmacokinetics and pharmacodynamics of anticancer agents used in gynaecological oncology. CME J Gynecol Oncol. 2001:5–16.
9. Spratlin J, Sawyer MB. Pharmacogenetics of paclitaxel metabolism. Crit Rev Oncol Hematol. 2007; 61:222–9. [PubMed: 17092739]
10. Sonnichsen DS, Liu Q, Schuetz EG, Schuetz JD, Pappo A, Relling MV. Variability in human cytochrome P450 paclitaxel metabolism. J Pharmacol Exp Ther. 1995; 275:566–75. [PubMed: 7473140]
11. Wensing KU, Ciarimboli G. Saving ears and kidneys from cisplatin. Anticancer Res. 2013; 33:4183–8. [PubMed: 24122981]
12. Maeda H. The enhanced permeability and retention (EPR) effect in tumor vasculature: the key role of tumor-selective macromolecular drug targeting. Adv Enzym Regul. 2001; 41:189–207.
13. Noguchi Y, Wu J, Duncan R, Strohalm J, Ulbrich K, Akaike T, et al. Early phase tumor accumulation of macromolecules: a great difference in clearance rate between tumor and normal tissues. Jpn J Cancer Res. 1998; 89:307–14. [PubMed: 9600125]
14. Oberoi HS, Nukolova NV, Kabanov AV, Bronich TK. Nanocarriers for delivery of platinum anticancer drugs. Adv Drug Deliv Rev. 2013; 65:1667–85. [PubMed: 24113520]
15. Desale SS, Cohen SM, Zhao Y, Kabanov AV, Bronich TK. Biodegradable hybrid polymer micelles for combination drug therapy in ovarian cancer. J Control Release. 2013; 171:339–48. [PubMed: 23665258]
16. Song W, Tang Z, Zhang D, Zhang Y, Yu H, Li M, et al. Anti-tumor efficacy of c(RGDfK)-decorated polypeptide-based micelles co-loaded with docetaxel and cisplatin. Biomaterials. 2014; 35:3005–14. [PubMed: 24388813]
17. Xiao H, Song H, Zhang Y, Qi R, Wang R, Xie Z, et al. The use of polymeric platinum(IV) prodrugs to deliver multinuclear platinum(II) drugs with reduced systemic toxicity and enhanced antitumor efficacy. Biomaterials. 2012; 33:8657–69. [PubMed: 22938766]
18. Kolishetti N, Dhar S, Valencia PM, Lin LQ, Karnik R, Lippard SJ, et al. Engineering of self-assembled nanoparticle platform for precisely controlled combination drug therapy. Proc Natl Acad Sci U S A. 2010; 107:17939–44. [PubMed: 20921363]
19. Xiao H, Li W, Qi R, Yan L, Wang R, Liu S, et al. Co-delivery of daunomycin and oxaliplatin by biodegradable polymers for safer and more efficacious combination therapy. J Control Release. 2012; 163:304–14. [PubMed: 22698937]
20. Xiao H, Song H, Yang Q, Cai H, Qi R, Yan L, et al. A prodrug strategy to deliver cisplatin(IV) and paclitaxel in nanomicelles to improve efficacy and tolerance. Biomaterials. 2012; 33:6507–19. [PubMed: 22727463]
21. Wang LH, Li Y, Yang SN, Wang FY, Hou Y, Cui W, et al. Gambogic acid synergistically potentiates cisplatin-induced apoptosis in non-small-cell lung cancer through suppressing NF-kappaB and MAPK/HO-1 signalling. Br J Cancer. 2014; 110:341–52. [PubMed: 24300974]
22. Luo J, Xiao K, Li Y, Lee JS, Shi L, Tan YH, et al. Well-defined, size-tunable, multifunctional micelles for efficient paclitaxel delivery for cancer treatment. Bioconjug Chem. 2010; 21:1216–24. [PubMed: 20536174]
23. Xiao K, Luo J, Fowler WL, Li Y, Lee JS, Xing L, et al. A self-assembling nanoparticle for paclitaxel delivery in ovarian cancer. Biomaterials. 2009; 30:6006–16. [PubMed: 19660809]
24. Song A, Wang X, Zhang J, Marik J, Lebrilla CB, Lam KS. Synthesis of hydrophilic and flexible linkers for peptide derivatization in solid phase. Bioorg Med Chem Lett. 2004; 14:161–5. [PubMed: 14684320]
25. Hoyle CE, Bowman CN. Thiol–ene click chemistry. Angew Chem Int Ed. 2010; 49:1540–73.
26. Chou TC. Theoretical basis, experimental design, and computerized simulation of synergism and antagonism in drug combination studies. Pharmacol Rev. 2006; 58:621–81. [PubMed: 16968952]
27. Chou TC, Talalay P. Quantitative analysis of dose-effect relationships: the combined effects of multiple drugs or enzyme inhibitors. Adv Enzym Regul. 1984; 22:27–55.

28. King FG, Dedrick RL. Physiological pharmacokinetic parameters for cisdichlorodiammineplatinum(II) (DDP) in the mouse. J Pharmacokinet Biopharm. 1992; 20:95–9. [PubMed: 1588505]
29. Kaiser E, Colescott RL, Bossinger CD, Cook PI. Color test for detection of free terminal amino groups in the solid-phase synthesis of peptides. Anal Biochem. 1970; 34:595–8. [PubMed: 5443684]
30. Huynh VT, Chen G, de Souza P, Stenzel MH. Thiol-yne and thiol-ene “click” chemistry as a tool for a variety of platinum drug delivery carriers, from statistical copolymers to crosslinked micelles. Biomacromolecules. 2011; 12:1738–51. [PubMed: 21476525]
31. Bastiat G, Pritz CO, Roider C, Fouchet F, Lignieres E, Jesacher A, et al. A new tool to ensure the fluorescent dye labeling stability of nanocarriers: a real challenge for fluorescence imaging. J Control Release. 2013; 170:334–42. [PubMed: 23792117]
32. Jekunen AP, Christen RD, Shalinsky DR, Howell SB. Synergistic interaction between cisplatin and taxol in human ovarian carcinoma cells in vitro. Br J Cancer. 1994; 69:299–306. [PubMed: 7905279]
33. Horvath V, Blanarova O, Svihalkova-Sindlerova L, Soucek K, Hofmanova J, Sova P, et al. Platinum(IV) complex with adamantylamine overcomes intrinsic resistance to cisplatin in ovarian cancer cells. Gynecol Oncol. 2006; 102:32–40. [PubMed: 16364413]
34. Eckstein N, Servan K, Hildebrandt B, Politz A, von Jonquieres G, Wolf-Kummeth S, et al. Hyperactivation of the insulin-like growth factor receptor I signaling pathway is an essential event for cisplatin resistance of ovarian cancer cells. Cancer Res. 2009; 69:2996–3003. [PubMed: 19318572]
35. Zhang Y, Huo M, Zhou J, Xie S. PKSolver: an add-in program for pharmaco-kinetic and pharmacodynamic data analysis in Microsoft Excel. Comput Methods Programs Biomed. 2010; 99:306–14. [PubMed: 20176408]
36. Alexis F, Pridgen E, Molnar LK, Farokhzad OC. Factors affecting the clearance and biodistribution of polymeric nanoparticles. Mol Pharm. 2008; 5:505–15. [PubMed: 18672949]
37. Gabizon AA. Pegylated liposomal doxorubicin: metamorphosis of an old drug into a new form of chemotherapy. Cancer Invest. 2001; 19:424–36. [PubMed: 11405181]
38. Vail DM, Kravis LD, Cooley AJ, Chun R, MacEwen EG. Preclinical trial of doxorubicin entrapped in sterically stabilized liposomes in dogs with spontaneously arising malignant tumors. Cancer Chemother Pharmacol. 1997; 39:410–6. [PubMed: 9054954]

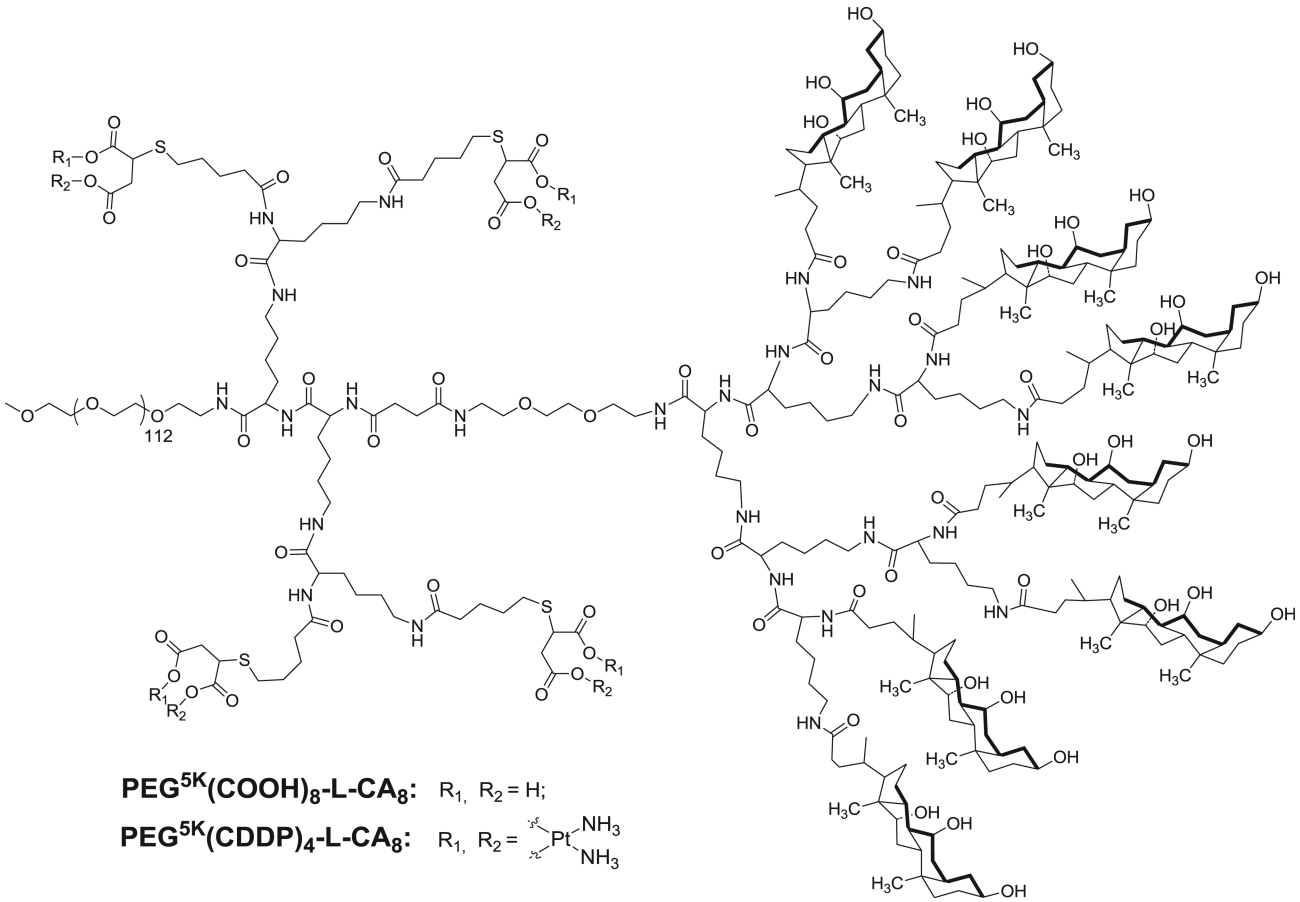

Scheme 1.

The structure of telodendrimer $PEG^{5K}(COOH)_8$-L-CA_8.

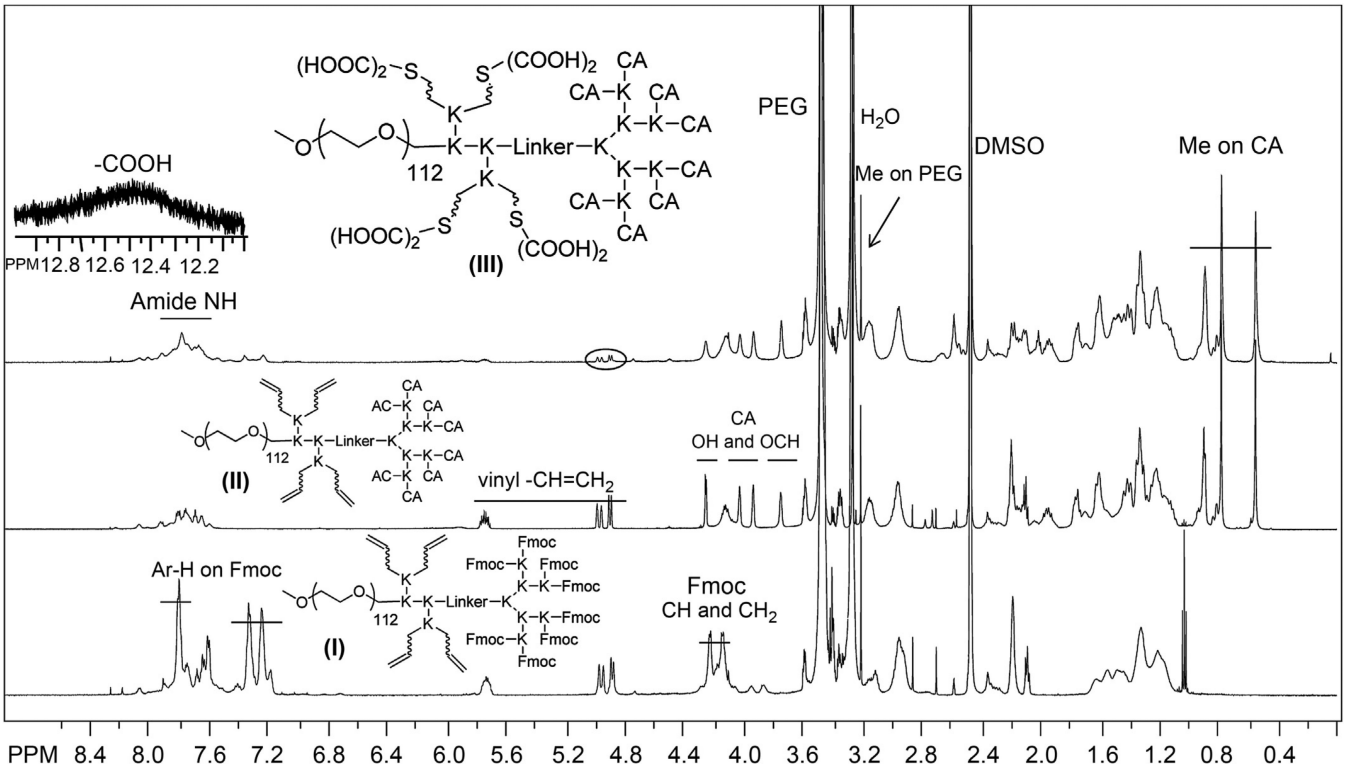

Fig. 1.

^{1}H NMR spectra of telodendrimer I, II and III in DMSO-d6 at a concentration of 5 mg/mL, detected by 600M Bruker NMR. The protons on Fmoc were marked in telodendrimer I; OH and OCH of CA and vinyl protons appeared in telodendrimer II; the Me of CA and emerging COOH and disappearing vinyl groups were shown in telodendrimer III.

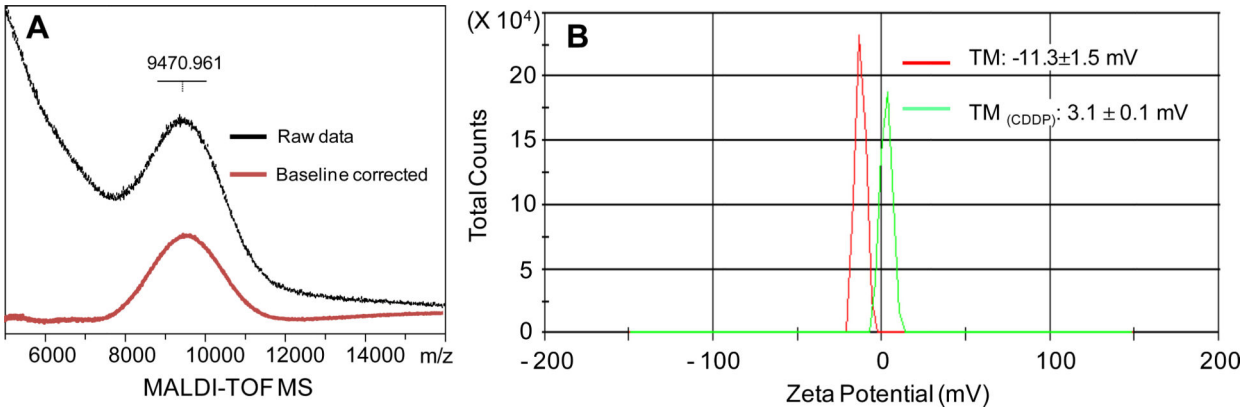

Fig. 2.

(A) MALDI-TOF MS spectrum of telodendrimer III (in black) with the baseline corrected (in red). (B) Zeta potential of telodendrimer III in red solid line and CDDP-loaded telodendrimer III in green solid line. (For interpretation of the references to colour in this figure legend, the reader is referred to the web version of this article.)

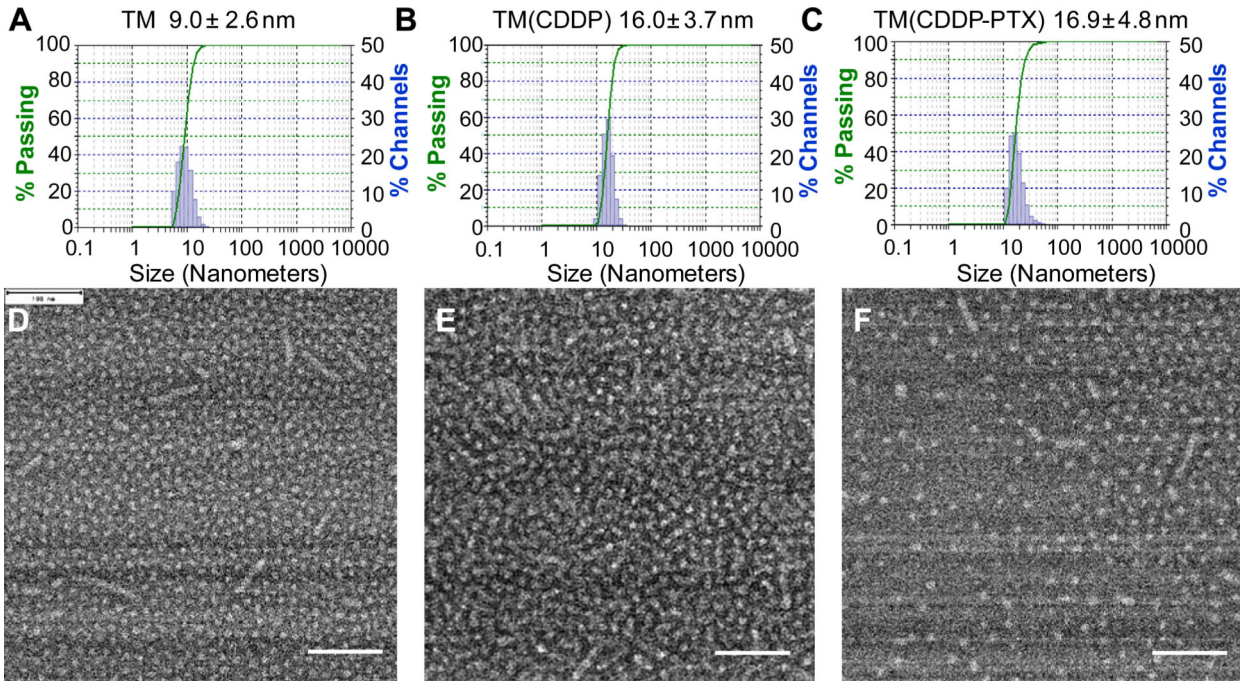

Fig. 3.

DLS particle sizes and TEM images of the empty TM (A, D) and single CDDP loaded TM (B, E) and PTX-CDDP co-loaded TMs (C, F). Scale bar: 100 nm.

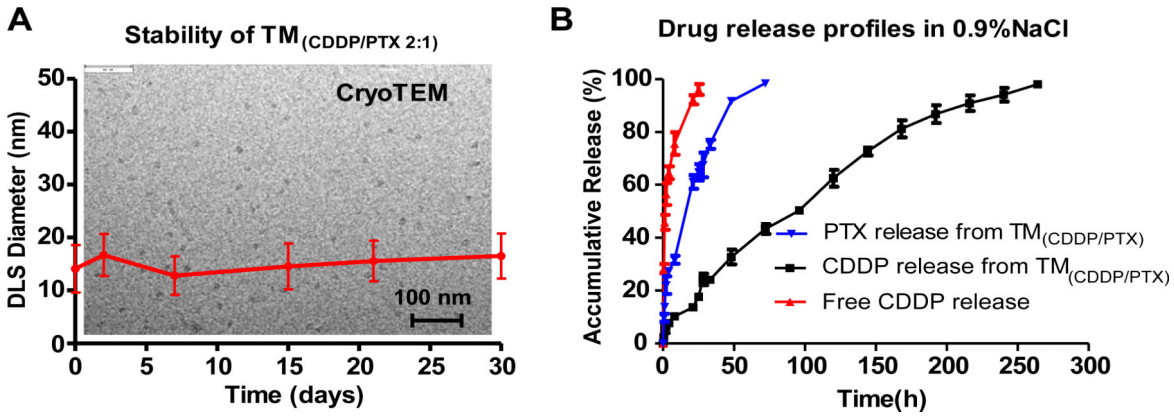

Fig. 4.

(A) DLS monitoring of particle size of $TM_{(CDDP/PTX\ 2:1)}$ micelle solution upon storage at 4 °C; The insert background is cryo-TEM image of the stored sample; (B) Drug release profiles of PTX and CDDP from the co-loaded nanoformulation in comparison with free CDDP.

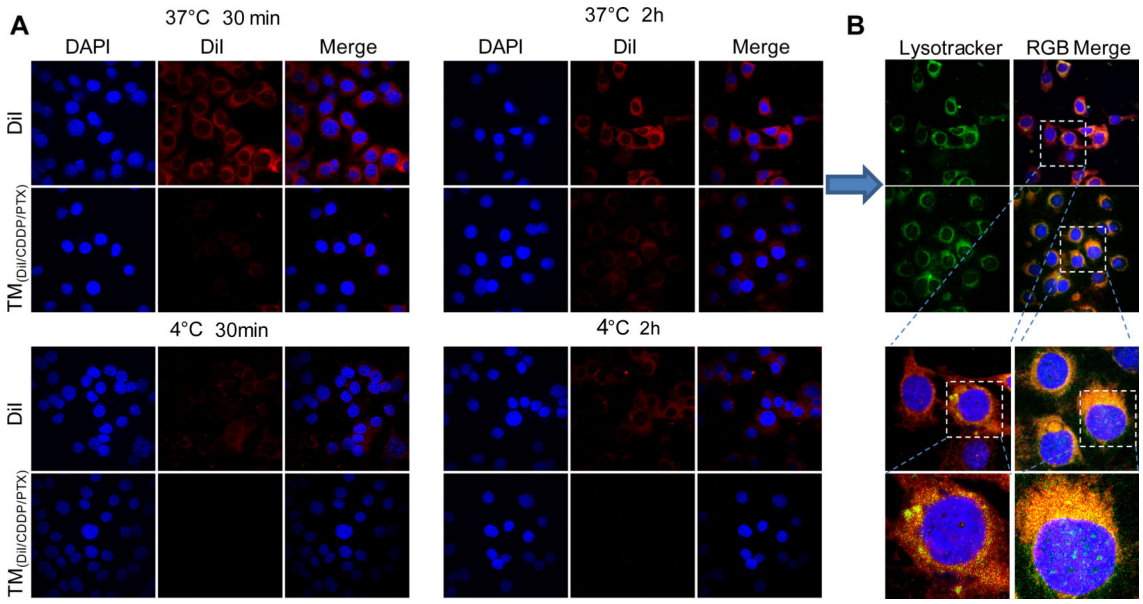

Fig. 5.

(A) Confocal fluorescence microscopy images of SKOV-3 cells incubated with free DiI and DiI-loaded micelles at 37 and 4 °C for 30 min and 2 h; (B) The overlay pictures of the cells incubated at 37 °C for 2 h cell nuclear and lysosome were stained with DAPI (Blue) and Lysotracker (green) respectively. (For interpretation of the references to colour in this figure legend, the reader is referred to the web version of this article.)

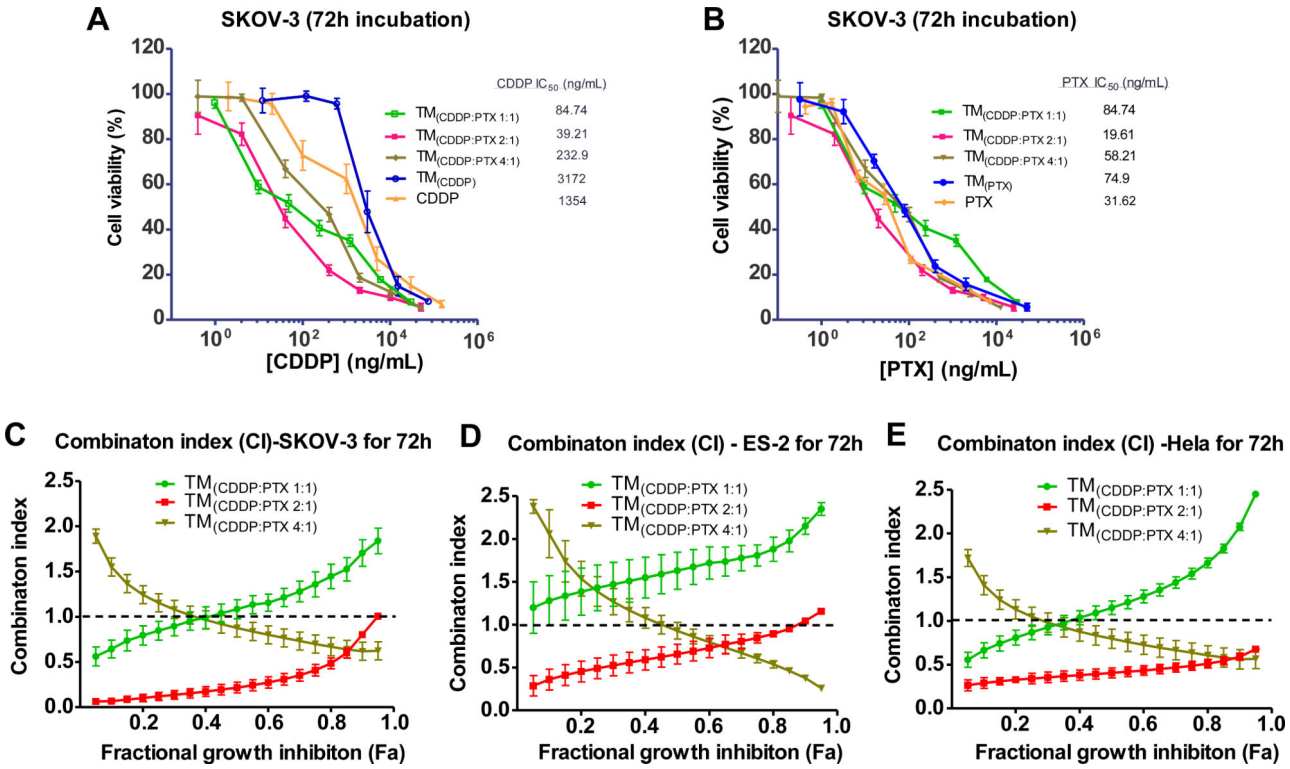

Fig. 6.

Cell viability of SKOV-3 ovarian cancer cells after incubated for 72 h with free CDDP, free PTX, single loading of $TM_{(PTX)}$ and $TM_{(CDDP)}$ and the coloading TM (CDDP:PTX0 at different ratios. The cell viabilities were displayed against PTX concentration (A) and CDDP concentration (B), respectively. The combination index of the co-loading TM formulations with different ratio of CDDP/PTX in SKOV-3(C), ES-2 cells (D) and in Hela cells (E).

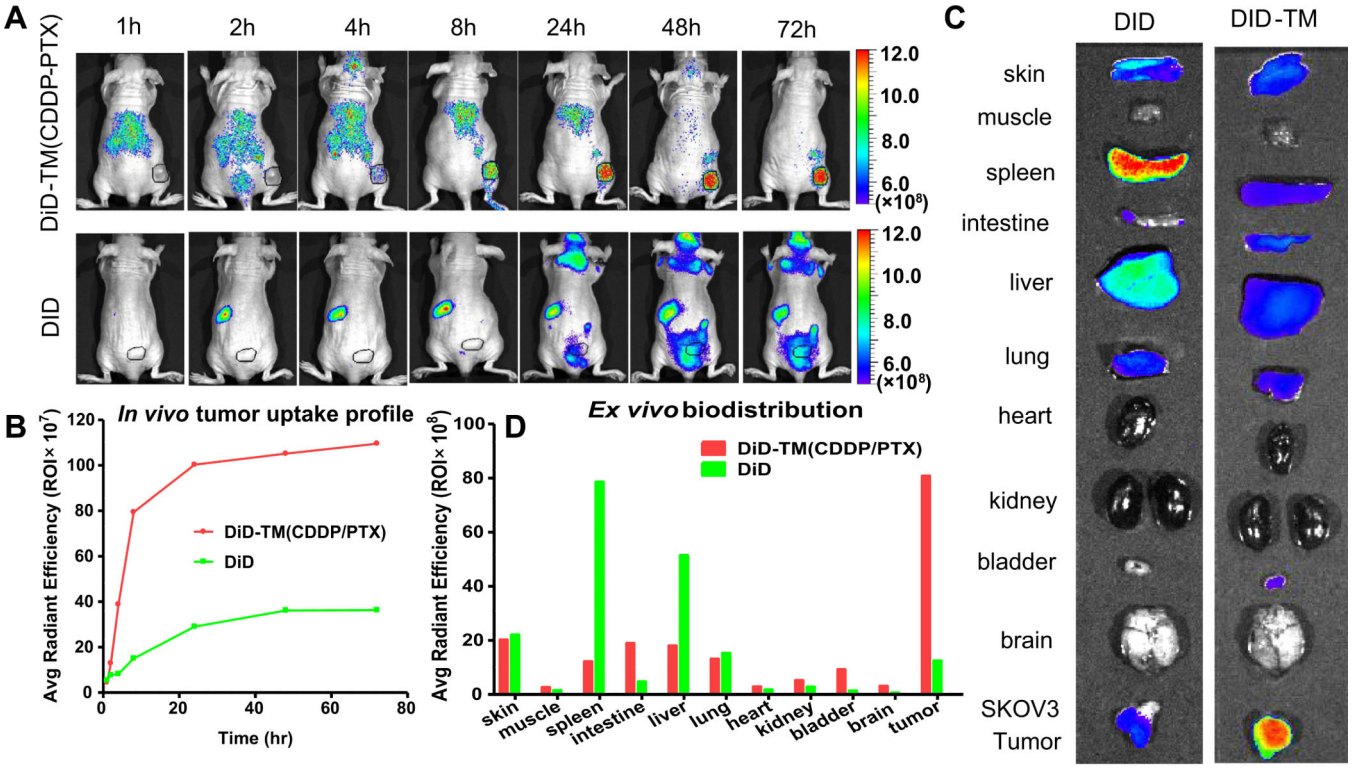

Fig. 7.

In vivo (A) and *ex vivo* (C) NIRF optical images of Raji lymphoma bearing mice injected intravenously with free DiD and DiD-PTX-CDDP coloaded TM formulations, respectively. The *in vivo* tumor targeting (B) and *ex vivo* tumor and organ uptake (D) were quantitatively analyzed.

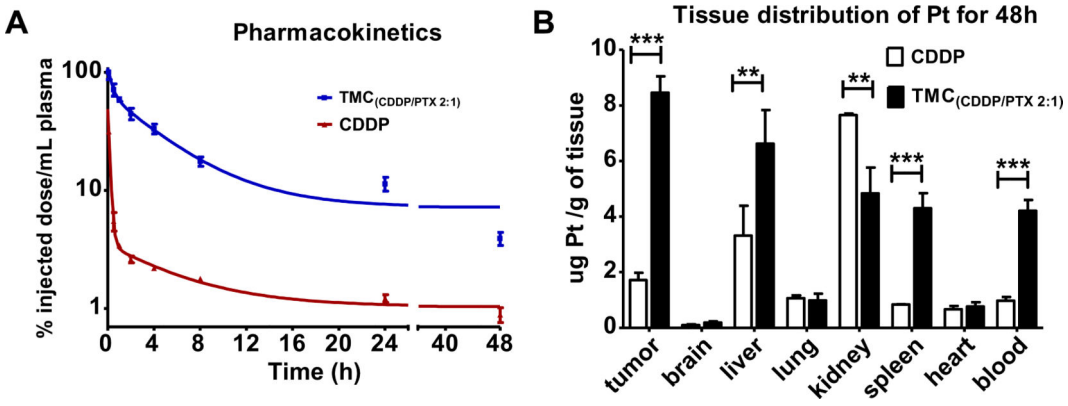

Fig. 8.

(A) *In vivo* pharmacokinetics profiles of platinum concentration in the plasma after i.v. administration of free CDDP and TM $_{(CDDP/PTX)}$. (B) Tissue distribution of platinum concentration in the plasma on day 2 after i.v. administration of free CDDP and PB-CDDP-PTX. Each drug was administered to Nude mice bearing human SKOV3 ovarian cancer tumor (female, $n = 3$) at a dose of 6 mg/kg on CDDP basis. Data were expressed as mean ± SE (**$p < 0.01$; ***$p < 0.005$).

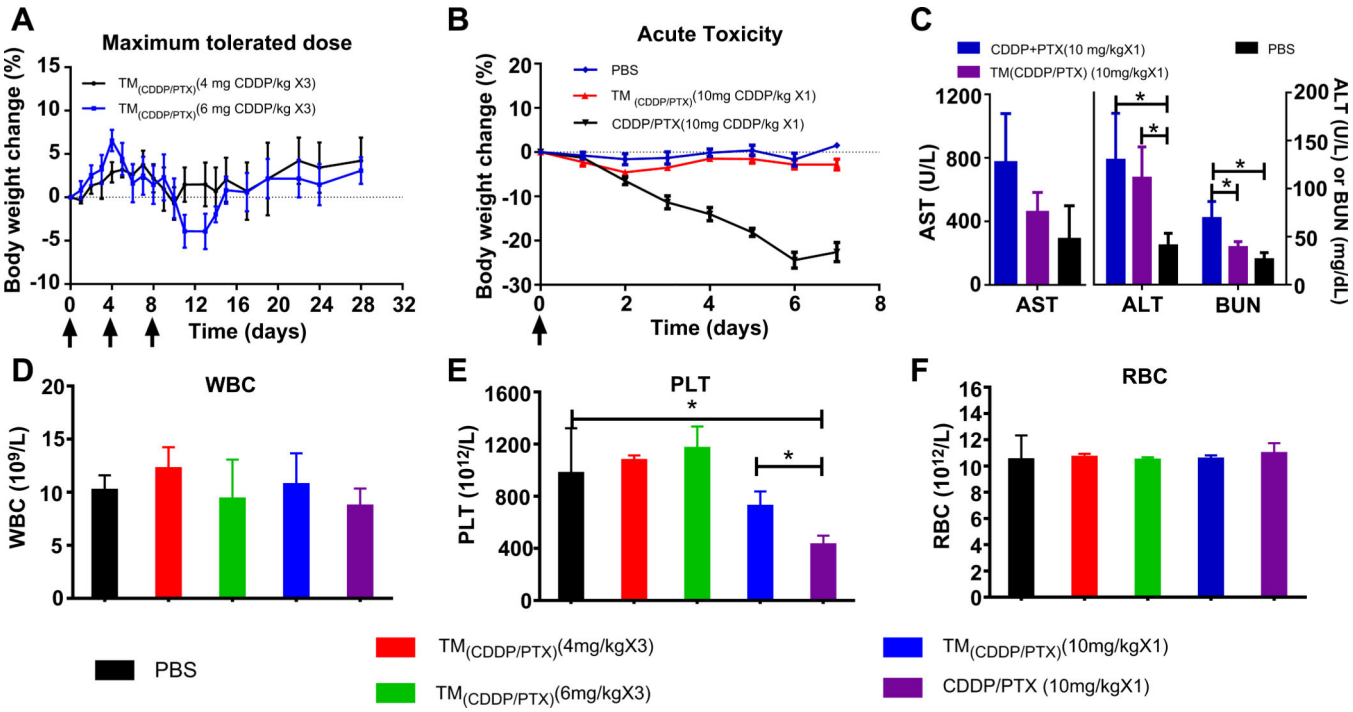

Fig. 9.

(A) The body weight changes for animals treated with $TM_{(CDDP/PTX = 2:1)}$ at two dosage levels, e.g. 4 and 6 mg CDDP/kg for three dosage in MTD study; (B) the body weight changes of animals treated with a single dose of free drug mixture of CDDP/PTX 2:1 w/w and $TM_{(CDDP/PTX = 2:1)}$ at 10 mg CDDP/kg level in comparison with PBS control group; (C) the serum AST and ALT enzyme levels and BUN level of animals in the acute toxicity studies treated with free CDDP/PTX and $TM_{(CDDP/PTX = 2:1)}$, respectively, at 10 mg CDDP/kg level; The blood cell counting analysis for WBC (D), PLT (E) and RBC (F) for the mice in MTD and acute toxicity studies. (*$p < 0.05$).

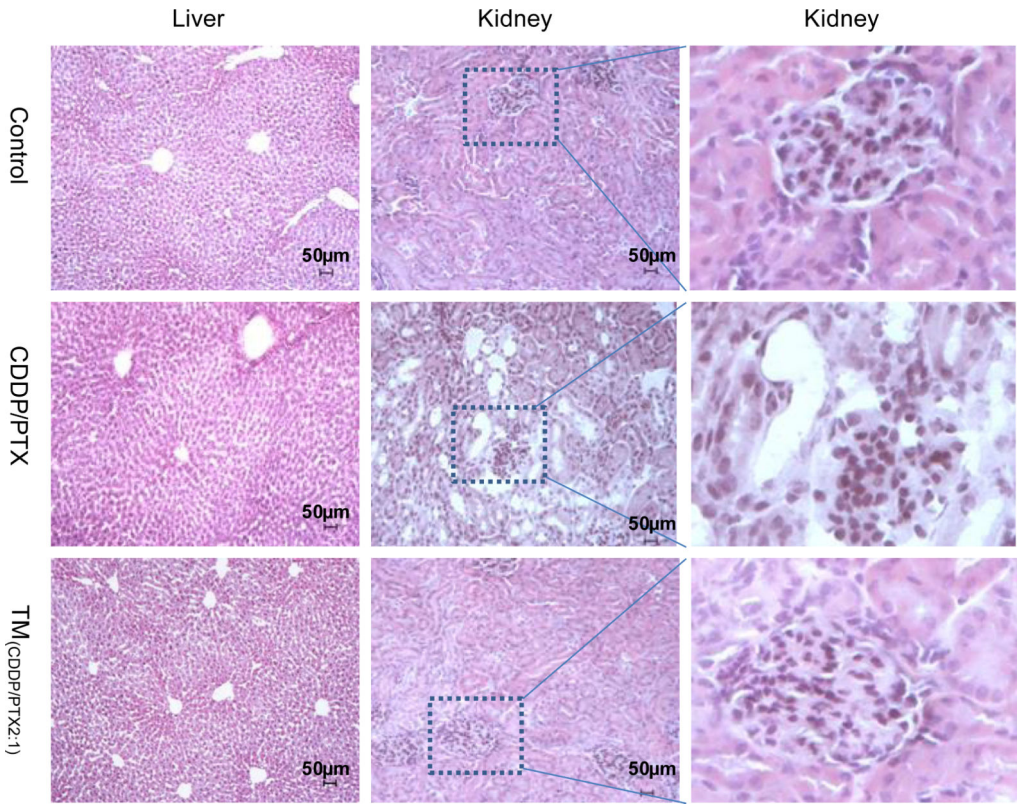

Fig. 10.

Histopathological changes in kidney and liver from the acute toxicity studies in BALB/c mice on day 7 after being treated with PBS (control), free CDDP/PTX and $TM_{(CDDP/\ PTX\ =\ 2:1)}$ at 10 mg CDDP/kg. Tissues were stained with fixed with 4% paraformaldehyde and stained with hematoxylin and eosin (H&E). Significant tubular dilation with flattening of the epithelium cells were observed only in the kidneys in mice treated with free CDDP/PTX mixture. No abnormal structures were observed in livers.

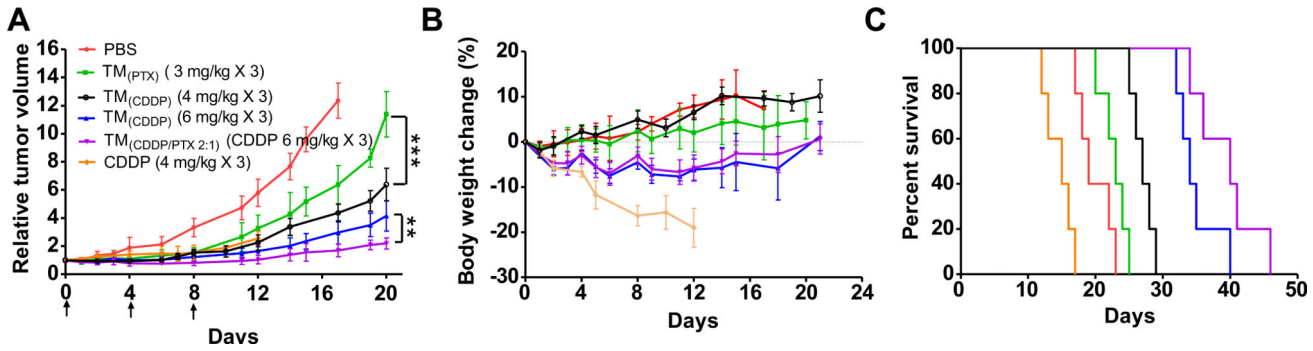

Fig. 11.

In vivo tumor growth inhibition (A), body weight changes (B) and KaplaneMeier survival curve (C) of mice beard SKOV-3 ovarian cancer xenografts ($n = 5$) after intravenous treatment with different CDDP and PTX formulations (on day 0, 4, 8). Figure B and C share the same legends with Figure A. (**$p < 0.01$; ***$p < 0.001$).

Table 1

Characterization and drug loading properties of telodendrimers

Formula (via NMR)	MW (Dalton)		CMC (μg/mL)	TM size (nm)	Size after drug loading (nm)		
	MS	Theo			$TM_{(PTX)}$	$TM_{(CDDP)}$	$TM_{(PTX\text{-}CDDP)}$
$PEG^{5k}COOH_{6.3}$-L-$CA_{6.2}$	9471	10,650	29.6	9.0 ± 2.6	16.0 ± 3.7	16.9 ± 3.7	16.9 ± 4.8

Table 2

IC50 and CI values of $TM_{(PTX/Pt)}$ with various PTX/Pt ratios.

Formulations	CDDP/PTX ratio (w/w)	SKOV-3		ES2		Hela	
		IC_{50} (ng/ml)	CI_{50}	IC_{50} (ng/mL)	CI_{50}	IC_{50} (ng/ml)	CI_{50}
CDDP		1354	–	920	–	2427	–
$TM_{(CDDP)}$		3172	–	1429	–	6765	–
PTX		32	–	55	–	20	–
$TM_{(PTX)}$		75	–	82	–	35	–
$TM_{(CDDP/PTX = 1:1)}$	1:1	85/85	1.16	126/126	1.62	40/40	1.15
$TM_{(CDDP/PTX = 2:1)}$	2:1	39/19.5	0.21	95/47.5	0.65	38/19	0.54
$TM_{(CDDP/PTX = 4:1)}$	4:1	233/58.3	0.87	242/60.5	0.91	109/27.3	0.79

Table 3

Pharmacokinetic parameter estimations of platinum in plasma of nude mice beard SKOV-3 xenograft after being treated with CDDP and $_{TM(CDDP/PTX)}$ through tail vein.[a]

<!–Col Count:3– > Parameters	$TM_{(CDDP/PTX)}$	CDDP
$t_{1/2}\alpha$ (h)	0.72	0.044
$t_{1/2}\beta$ (h)	12.36	4.30
C_{max} [b] (μg/mL)	88.02	27.58
CL (mL/kg/h)	6.38	129.87
CL2 (mL/kg/h)	22.35	559.30
AUC (μg/ml*h)	627.44	30.80
V_{ss} (mL/kg)	103.55	668.10

[a] The pharmacokinetic parameters were calculated using a two compartment model with PKsolver, an add-in program in Microsoft Excel [35].

[b] C_{max} represents the maximum observed concentration at the earliest evaluated time point of 5 min post *iv* injection; Plasma concentration at 0 h time point were calculated based on the dose of 4 mg/kg. Abbreviations: $t_{1/2}$, half life time; C_{max}, maximum platinum concentration; AUC, area under the curve; Cl, clearance; V_{SS}, steady-state volume of distribution.